

Microscopic aspects of crack propagation along PET–glass and PET–Al interfaces

W.P. Vellinga ^{*}, R. Timmerman, R. van Tijum, J.Th.M. De Hosson

*Department of Applied Physics, Materials Science Centre and the Netherlands Institute for Metals Research,
University of Groningen, Nijenborgh 4, 9747 AG Groningen, The Netherlands*

Received 7 October 2005; received in revised form 28 March 2006

Available online 11 May 2006

Communicated by Thomas Pardoen

Abstract

This paper reports microscopic investigations of the propagation of cracks along polymer–glass and polymer–metal interfaces. The experimental methods include an asymmetric double cantilever beam in an optical microscope, and birefringence and atomic force microscopy of the crack faces. The crack fronts propagate inhomogeneously in space and time by way of forward bursts that spread laterally along the front over a certain distance. Experimental indications for correlation between crack propagation and interface roughness and for the occurrence of shear-bands in front of the propagating interface cracks are discussed.

© 2006 Elsevier Ltd. All rights reserved.

Keywords: Polymer–metal interfaces; Interface cracks; Delamination; Crack propagation; Microscopy

1. Introduction

Polymer–metal interfaces appear in applications as diverse as beverage cans and high-tech displays. The lifetime of such applications is usually limited by crack propagation along the polymer–metal interfaces. There is growing interest in combining concepts from continuum mechanics (stresses, stress intensity factors, energy release rates) with ideas from statistical physics (interplay between disorder and stress-aided thermally activated processes (e.g. Santucci et al., 2004)) to obtain lifetime predictions. In crack initiation and propagation locally stored elastic energy is released through the formation of a crack surface, generation of heat, and possibly associated irreversible plastic deformation. This means that local fluctuations in geometry, such as layer thickness, interface bonding or material properties may contribute to disorder in the local energy release rate associated with the interface crack. Recently, experiments on cracks propagating along weak PS–PS interfaces have revealed scaling behavior of crack front shape and crack front dynamics (Schmittbuhl, 1997; Måløy

^{*} Corresponding author. Tel.: +31 503634821.

E-mail address: w.p.vellinga@rug.nl (W.P. Vellinga).

et al., 2003). The degree of disorder, local stress concentrations near irregularities on the front, or elastic interaction (potentially of long range character) along the front are all expected to influence the crack shape and crack dynamics (for a review see e.g. (Bouchaud, 2003)).

We present microscopic observations on the propagation of cracks along polymer–glass and polymer–metal interfaces and focus on microscopic aspects of the propagation mechanism.

2. Experimental

The experimental method employed is an asymmetric double cantilever beam (ADCB) test (for a schematic picture see Fig. 1) mounted on a miniature tensile stage which fits in a reflection optical microscope. Driving speeds for the cracks are of the order of 10 $\mu\text{m/s}$. Samples consist of glassy poly-ethylene terephthalate (PETG) spin-coated on steel, with a thickness of 15 μm , or PETG spin-coated on Al with a thickness of 15 μm .

The samples are dried at 80 $^{\circ}\text{C}$ for a few hours, and subsequently pressure bonded to a glass support (for 240 s, at 140 $^{\circ}\text{C}$ and 1.5 MPa). In the experiment a crack may propagate along the PETG–glass interface as well as along the rough and anisotropic (ridges in the rolling direction) PETG–metal interface (rms $\sim 1 \mu\text{m}$). The crack front is observed through the glass with a CCD camera (1376 \times 1032 pixels, 3 \times 8 bit) at a rate of 1 Hz.

For details on ADCB experiments and related issues reference is made to (Hutchinson and Suo, 1992; Bernard et al., 1999). In practice $a \gg h_1, h_2$. Also at all times, for the remaining adhered portion of the beam $L, L \gg a$ should hold. In ADCB the energy release rate G is determined by measuring a and using the approximate formulae shown below (Bernard et al., 1999):

$$G = \frac{(3\Delta^2 E_1 E_2 h_1^3 h_2^3)(C_2^2 E_1 h_1^3 + C_1^2 E_2 h_2^3)}{8a^4 \Lambda^2} \quad (1)$$

with $\Lambda = C_1^3 E_2 h_2^3 + C_2^3 E_1 h_1^3$ and $C_i = 1 + 0.64 \frac{h_i}{a}$.

An example of an unprocessed image with high brightness but low contrast near the crack front is shown in Fig. 2-I. In the experiment the position of the knife is fixed, and the sample is clamped in one of the clamps of the tensile stage. The movement of the clamps may not be entirely smooth, or aligned perfectly with the coordinate system of the image. Standard image correlation techniques allow determination of the movement of the sample between two images, and so the movement of the front with respect to the sample during the same time can be determined, (see for example Fig. 2-Ia).

Subsequently, depending on the contrast and brightness (that may be influenced by the use of crossed polarizers) several image processing steps may be required to determine the front position. For images with high brightness and low contrast in the front region such as shown in Fig. 2, in order to isolate the fronts we subtract two images that are n frames apart (Fig. 2-II). If the correlation is good this gets rid of the background effectively. The main stages in the determination of the front position are shown in Fig. 2-III and -IV. The subtraction image is noise filtered and thresholded, which leaves a solid area behind the front. However, the front usually shows holes (Fig. 2-III). Either the front may not or hardly have moved in the time lapse between the acquisition of the two images (*intrinsic* hole), or the displacement vector from correlation is in

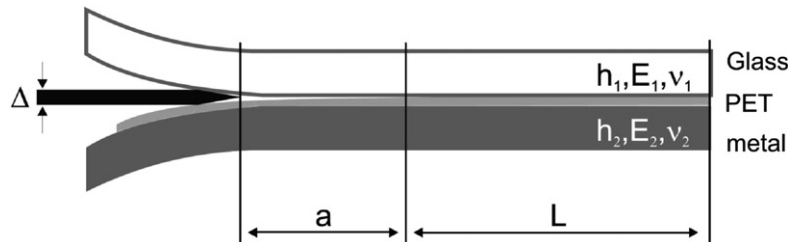


Fig. 1. Schematic drawing of an ADCB experiment. A razor blade (black) is inserted between PET and glass (shown) or PET and metal. Δ crack opening, a crack length, L uncracked length. h_i height, E_i Young's modulus, ν_i Poisson's ratio, subscript $i = 1, 2$ refer to glass, metal respectively.

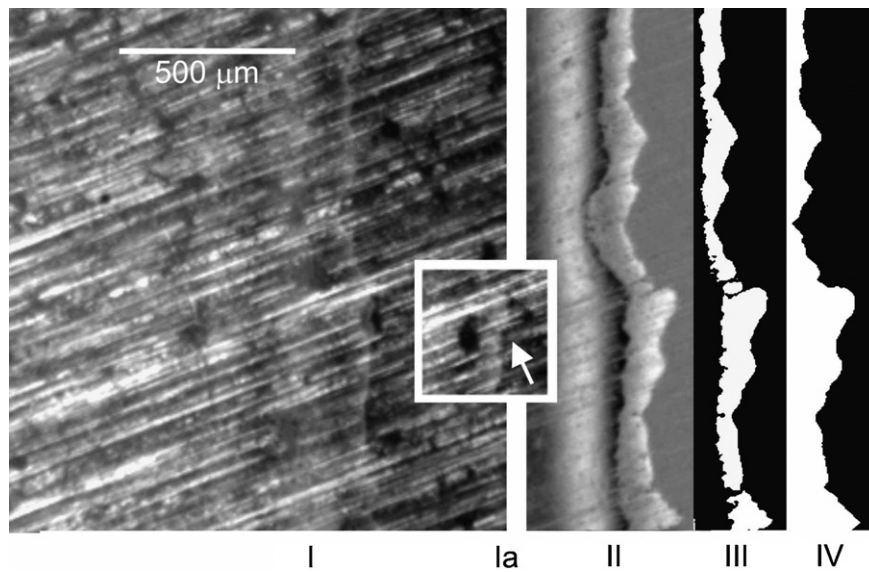


Fig. 2. Laminate 1, image processing I: Image I_0 at t_0 , showing metal roughness, wedge fringes where laminate has separated (left), brightness change at crack front. Ia: Part of image I_{30} at $t_0 + 30$ (s). Arrow represents exaggerated displacement vector necessary to bring background into registry. II: Pixel-wise subtraction $I_{30} - I_0$ after image registration. III: Thresholding. IV: Front filling (see text).

error, which combined with the background texture leads to missing lines (*extrinsic* holes). To fill intrinsic holes we take the last front position that was successfully calculated. The same procedure is used for the extrinsic holes. Denoting thresholded images by T and front files by C the following is therefore performed in a pixel-wise fashion,

$$C_{i+1} = \text{OR}(T_{i+1}, C_i) \quad (2)$$

Subsequently the image behind the front is filled (Fig. 2-IV), and noise ahead of the front removed using an opening operator. Finally the front itself is isolated subtracting an eroded version of the image from itself.

For images with low brightness but with more contrast in the region of the crack front, typical for images taken between crossed polarizers, image subtraction may be impractical because of the decrease of the signal-to-noise ratio. However in these cases the front region usually has a distinct color (hue), which can be separated out. In many cases these fronts show holes that are filled in the same way as for the other type of images by incrementally adding new front locations starting from an initial complete front using a bitwise OR operation.

3. Results and discussion

Results of experiments carried out on three different laminates are shown in Fig. 3 (laminate 1), Fig. 4 (laminate 2) and Figs. 5 and 6 (laminate 3). In laminates 1 and 3 the crack was found to propagate essentially along the PET–glass interface, in laminate 2 propagation occurred along the PET–Al interface. The front shown in Fig. 3 was moving at a constant mean speed of $5 \mu\text{m/s}$, the front shown in Fig. 4 was slowly accelerating and the front shown in Figs. 5 and 6 was moving spontaneously (and slowing down) after the knife had been stopped some time before.

The main observation in Figs. 3–6 is that on a microscopic scale the crack propagation is inhomogeneous *in time* as well as *in space*: parts of the front become unstable and move ahead of the mean crack position.

In Fig. 3 such instabilities in the front are subsequently seen to spread laterally along the front for some distance, with a clear preferred direction, upward in the figure. Also weak spatial correlations in the position of the forward bursts can be observed, apparent e.g. from the directionality in the observed spatiotemporal burst pattern. We speculate that local differences in the energy release rate related to the thickness differences

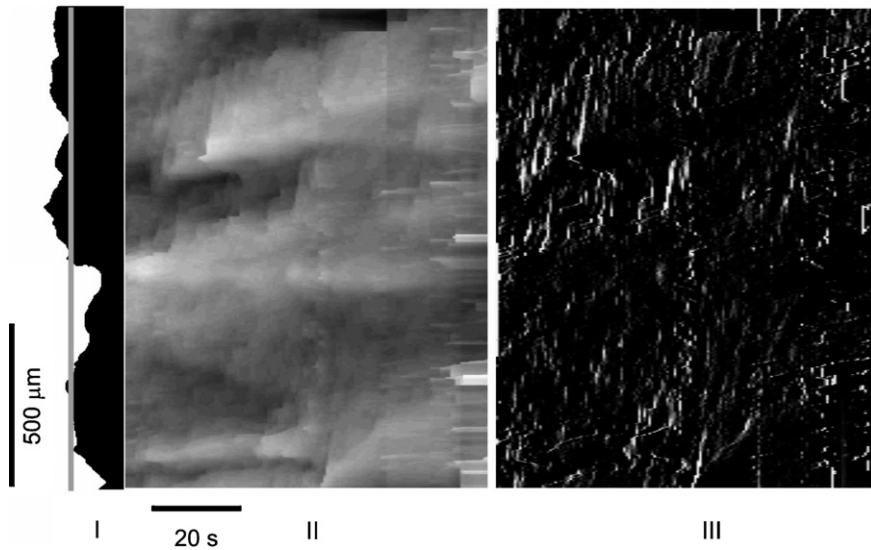


Fig. 3. I: Laminate 1. Grey line indicates the mean front position \bar{x} . II: $\Delta x_i(t) = x_i(t) - \bar{x}(t)$, light parts: $x_i(t) > \bar{x}(t)$, dark parts: $x_i(t) < \bar{x}(t)$. III: Forward “acceleration” $\Delta x(t)/\Delta t$ (with $\Delta t = 1(s)$) as a function of time and position along front. $G = 2 \text{ J/m}^2$.

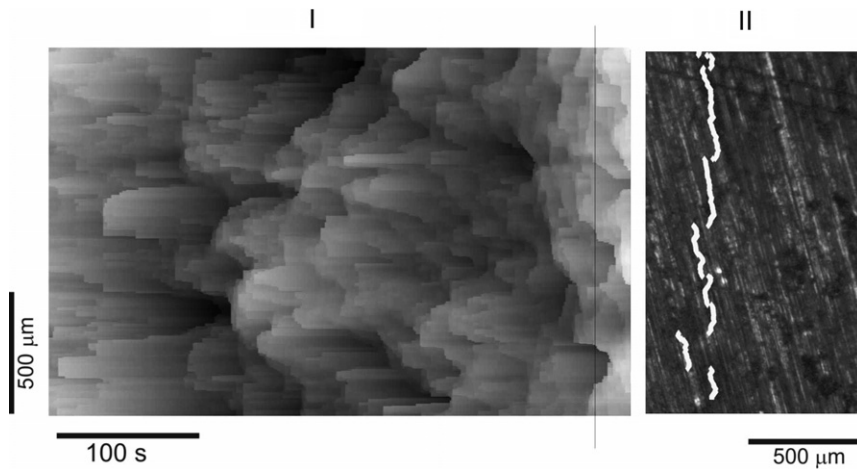


Fig. 4. Laminate 2. I: $\Delta x_i(t) = x_i(t) - \bar{x}(t)$. II: Snapshot of front at position of the black line indicated in I the front position was determined as outlined in the text and superimposed on a grayscale version of the original image. Note the alignment of parts of the front with the ridges on the metal surface.

associated with the ridges on the metal are responsible for both these weak correlations, as well as for the preferred direction in the burst movement.

Qualitatively similar behavior was encountered for cracks propagating along PET–metal interfaces as is evident from Fig. 4-I. A snapshot of the front position is shown in Fig. 4-II, together with part of a raw image that serves to illustrate the metal surface topography. Alignment of parts of the front with the ridges on the metal surface is evident, establishing a clear correlation between crack propagation and interface topography or disorder.

Figs. 5 and 6 illustrate an essentially similar but more extreme mode of crack propagation. In this case the lateral movement associated with an instability may span the entire sample width. In fact the forward movement of the crack front consists almost entirely of lateral movement of forward steps along the front, i.e. a mechanism similar to double-kink motion of dislocations in bcc metals. However, from Fig. 5-II it is clear that

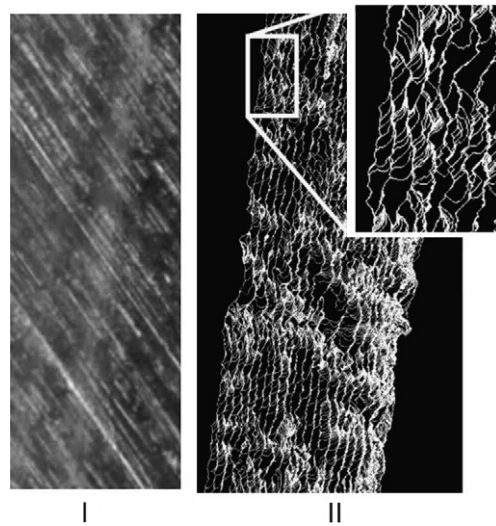


Fig. 5. I: Snapshot of front in laminate 3. II: Approximately 400 subsequent front positions. Front movement is mainly due to bursts parallel to the front as shown in the inset. $G = 4 \text{ J/m}^2$.

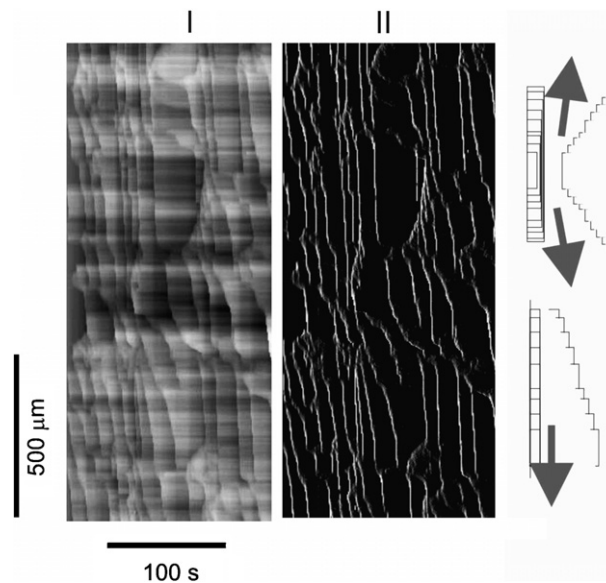


Fig. 6. Propagation of front in laminate 3. I: $\Delta x_i(t) - x_i(0)$. II: $\Delta x_i(t)/\Delta t$ (with $\Delta t = 1(s)$). $G = 4 \text{ J/m}^2$. The appearance of two different propagation phenomena is illustrated in the sketch drawings.

forward bursts do also occur, and that a strong spatial correlation exists between the position of a burst with that of a subsequent burst.

Another remarkable feature of the movement shown in Figs. 5 and 6 is the occurrence of a characteristic forward step size. A similar phenomenon has been noted for cracks propagating along epoxy–glass interfaces (Swadener et al., 1999). We note that in the literature arrays of regularly spaced shear bands have been observed in front of cracks propagating along interfaces between glassy polymers (Bernard et al., 1999) which could well be responsible for the characteristic step size. To further investigate the possibility of the occurrence of shear bands in the crack front region two microscopic techniques were employed, tapping mode AFM and polarization (birefringence) microscopy. Images made with these techniques are shown in Fig. 7.

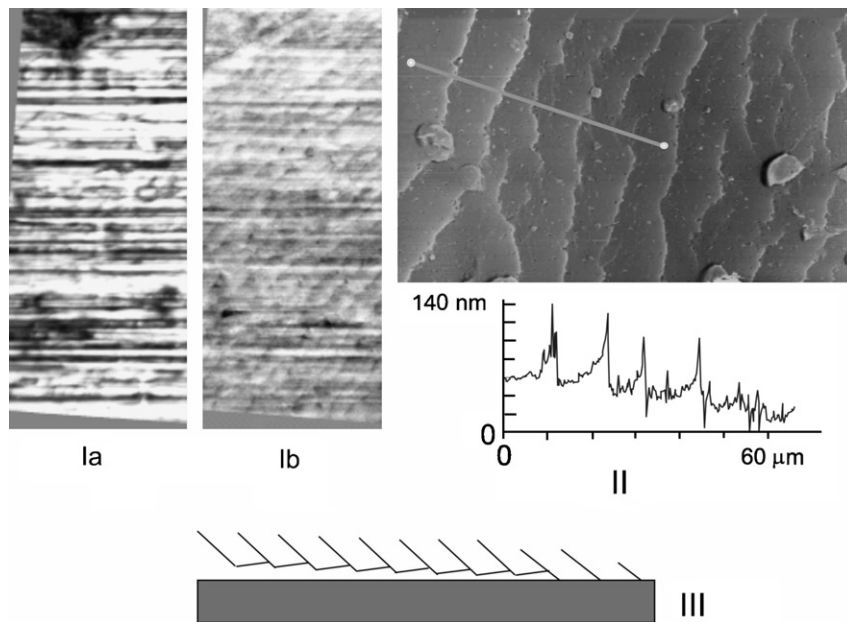


Fig. 7. Microscopic images of PET crack surface in laminate 3. Ia and Ib: Birefringence microscopy. Ia: local image intensity. Ib: Local birefringence. Note array of lines in Ib. II: Tapping mode height image of the same surface (at higher magnification and slightly turned). Inset shows profile along line indicated in image. Note array of ridges. III: Sketch of presumed mechanism leading to the surface relief: shear bands form ahead of the crack tip, on delamination release of constraints leads to deformation around these bands.

The AFM measurements were performed on the PET crack surface. Ridges of about 150 nm height can be seen with an interdistance of the order of 15 μm , which corresponds very well with the distance between the crack fronts as derived from the front propagation measurements. The ridges are curved but on a length-scale much smaller their interdistance the crack surface is quite smooth. The glass countersurface did not show any similar patterns, or comparable surface relief and it is concluded that the ridges must be predominantly due to irreversible remnant deformation of the PET. The presence of irreversible deformation is confirmed by polarization microscopy. Many glassy polymers show optical birefringence upon deformation. The method used to image birefringence in PET is due to Glazer (Glazer et al., 1996) adapted for use in reflection microscopy. (This requires only minor deviations from the theory described in (Glazer et al., 1996) and this will be discussed in more detail elsewhere (van Tijum et al. in preparation).) Qualitative results in Fig. 7 show the local image intensity and birefringence. The birefringence image shows a pattern of lines consistent with the surface features in the AFM measurements, and it is concluded that those are indeed associated with remnant irreversible deformation in the PET. The situation is consistent with earlier observations of regular arrays of shear bands in front of crack tips propagating along interfaces between glassy polymers. Fig. 7 shows a sketch of a possible geometry for such an array of shearbands forming ahead of the crack and reducing the stresses in the polymer away from the interface. More concentrated loads will exist at their “base” on the interface with the glass which may become a preferred path for delamination. The area between two bases may delaminate when the base of the shearband has de-adhered some distance. The deformation inside the shearband is irreversible, and as delamination occurs the material around the shearband (no longer constrained by the interface) will change shape to accommodate it.

4. Conclusions

In conclusion crack fronts moving along interfaces of PET layers confined between a glass and a metal surface were found to propagate inhomogeneously in space and time. The fronts move in forward bursts that spread laterally along the front. Qualitatively similar crack front propagation phenomena have been reported in the literature. Similar to Figs. 3 and 4 for polymer–polymer (PS–PS) interfaces (Schmittbuhl, 1997; Måløy

et al., 2003), and similar to Figs. 5 and 6 for epoxy–glass interfaces (Swadener et al., 1999). This seems to indicate that such crack front movement is in fact a quite common mechanism.

A correlation between crack front propagation with disorder – in this case the interface roughness or related thickness differences – in the confined layer was encountered, and was more obvious in a crack propagating along a rough surface.

The occurrence of a characteristic forward step size observed in some instances was shown to be characterized by a linear array of ridges at the crack surface due to permanent deformation in the PET. Evidence from AFM and birefringence microscopy lead to an explanation in terms of residual deformations due to the formation of an array of shearbands in front of the moving crack tip.

Acknowledgements

The authors would like to acknowledge financial support by IOP (project IOT 01001) and STW (project GTF 4901) and the help of Beltran de Jong with the birefringence microscopy.

References

- Bernard, B., Brown, H.R., Hawker, C.J., Kellock, A.J., Russell, T.P., 1999. Adhesion of polymer interfaces reinforced with random and diblock copolymers as a function of geometry. *Macromolecules* 32, 6254–6260.
- Bouchaud, E., 2003. The morphology of fracture surfaces: a tool to understand crack propagation in complex materials. *Surface Review and Letters* 10, 797.
- Glazer, A.M., Lewis, J.G., Kaminsky, W., 1996. An automatic optical imaging system for birefringent media. *Proceedings of the Royal Society of London A* 452, 2751–2765.
- Hutchinson, J.W., Suo, Z., 1992. Mixed mode cracking in layered materials. *Advances in Applied Mechanics* 29, 63–199.
- Måløy, K.J., Schmittbuhl, J., Hansen, A., Batrouni, G.G., 2003. Scaling and dynamics of an interfacial crack front. *International Journal of Fracture* 121, 9.
- Santucci, S., Vanel, L., Ciliberto, S., 2004. Subcritical statistics in rupture of fibrous materials: experiments and model. *Physics Review Letters* 93, 095505.
- Schmittbuhl, J., Måløy, K.J., 1997. Direct observation of self-affine crack propagation. *Physics Review Letters* 78, 3888–3891.
- Swadener, J.G., Liechti, K.M., de Lozanne, A.L., 1999. The intrinsic toughness and adhesion mechanism of a glass/epoxy interface. *Journal of Mechanics and Physics of Solids* 47, 223–258.